한국지반공학회논문집 제16권 제4호 2000년 8월 PP 191 ~199

Finite Element Analysis of Piezocone Test II

피에조콘 시험의 유한요소 해석 II

Kim, Dae-Kyu 김 대 규*1
Kim, Nak-Kyung 김 낙 경*2

요 지

본 연구에서는 피에조콘 시험의 유한요소 해석을 수행하였다. 이를 위하여 점탄소성 bounding surface 모델, 가상일의 방정식 (virtual work equation) 및 theory of mixtures를 Updated Lagrangian reference frame에서 formulation 하였다. 결과적으로 구성된 유한요소 formulation을 컴퓨터 프로그래밍 하였으며 유한요소해석에서 얻은 콘 저항치, 과잉간극수압 및 간극수압소산 등의 결과를 실험치와 비교 분석하였으며 피에조콘 주변의 응력, 변형율 및 과잉간극수압의 contour를 유한요소해석에서 구하여 이를 고찰하였다. 비등방성 및 점성이 추가된 구성모델을 사용함으로서 응력의 비등방성 및 관입속도를 효과적으로 simulation할 수 있었다. 유한요소Formulation 과정은 'Ⅰ', 결과는 'Ⅱ' 에서 설명된다.

Abstract

In this research, the finite element analysis of piezocone penetration and dissipation tests has been conducted using the anisotropic elastoplastic-viscoplastic bounding surface model, virtual work equation, and theory of mixtures formulated in the Updated Lagrangian reference frame for the large deformation and finite strain nature of piezocone penetration. The formulated equations have been implemented into a finite element program. The cone resistance, excess pore water pressure, and dissipation of excess pore water pressure from the finite element analysis have been compared and investigated with the experimental results. The contours of stress, strain, and excess pore water pressure near the piezocone have been also investigated. An effective simulation could be performed with the use of the anisotropic and viscous soil model. The finite element formulations and the results are described in part 'Ⅰ' and part 'Ⅱ', respectively.

Keywords : Bounding surface model, Piezocone, Updated lagrangian formulation

1. Introduction

In part 'Ⅰ' of this paper, the finite element formulation has been performed using the anisotropic elastoplastic-viscoplastic bounding surface model (Al-Shamrani and Sture, 1994), virtual work equation, and theory of mixtures (Prevost, 1980; Abu-Farsakh, et al., 1997) in the Updated Lagrangian reference frame to consider the anisotropy and penetration rate effects, and the large displacement and large deformation nature of piezocone penetration. The viscoplastic part of the soil model played the most important role in all the formulations. In this paper, the results of the finite element

*1 정회원, 고려대학교 방재과학기술연구센터 선임연구원
*2 정회원, 성균관대학교 공과대학 토목공학과 조교수

analysis of piezocone penetration mechanism are presented. The profiles of cone resistance and excess pore water pressure during the penetration test, and the dissipation of excess pore water pressure during the dissipation test are compared with the experimental results and the contours of stress, strain, and excess pore water pressure around the piezocone are investigated.

2. Computer Implementation and Numerical Simulation of Piezocone Penetration

The global coupled equation formulated in part ' I ' has been implemented into a computer program, EPVPCS-S (ElastoPlastic-ViscoPlastic Coupled System-Soil), based on Voyiadjis and Abu-Farsakh's work (1997). The piezocone penetration was treated as an axi-symmetric boundary problem and the piezocone penetrometer was assumed to be infinitely stiff. No tensile stresses were allowed to develop along the centerline boundaries. Since the soil around the piezocone penetrometer undergoes substantial displacements during penetration, a large displacement and finite strain formulation was used in the analysis. To avoid the tremendous computational errors in the transient state due to large rotations of the elements involved, the piezocone penetrometer was assumed to be initially pre-bored to a certain depth with the initial stresses remaining unchanged. The friction between the piezocone penetrometer and soil was considered using the constraint approach (Katona, 1983). The continuous penetration of piezocone was simulated by applying an incremental vertical displacement of the piezocone boundary (fig. 1). The vertical displacement could be applied at various rates but 0.3 cm/sec and 0.6 cm/sec were applied, which were the same rates at the piezocone penetration tests conducted using LSU/CALCHAS (Louisiana State University Calibration Chamber System).

In the calibration chamber test, six penetration and dissipation tests have been conducted using the U1 type (filter element at the very cone tip) and the U2 type (filter element 1mm above the cone base) miniature piezocone penetrometers, for normally consolidated and heavily overconsolidated (OCR=10) cohesive specimens, and at the penetration rates of 0.3 cm/sec and 0.6 cm/sec. Table 1 shows the piezocone penetration and dissipation test program. Details on the calibration chamber test are presented in Kim (1999).

The conditions of the above tests have been simulated in the finite element analysis. The results of the finite element

Table 1. Piezocone Penetration Test Program

Test no.	Filter location	σ_v (KPa)	σ_h (KPa)	Ko	OCR	Penetration Rate (cm/sec)
1	u1	262 01	110 04	0.42	1	0 3
2	u2	262 01	110 04	0.42	1	0 3
3	u1	262 01	110 04	0.42	1	0 6
4	u2	262 01	110 04	0.42	1	0 6
5	u2	26.20	41 40	1.58	10	0 6
6	u1	26.20	41.40	1.58	10	0.6

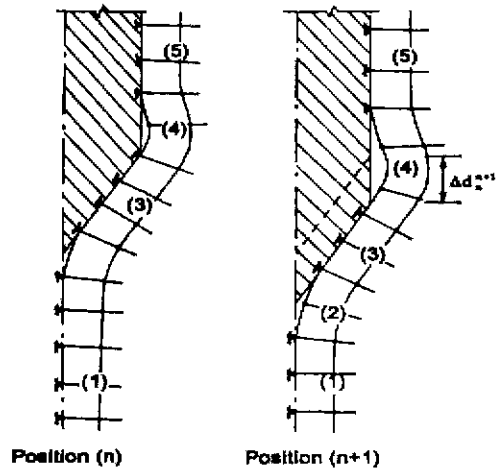

Fig. 1 Incremental Penetration (Voyiadjis and Abu-Farsakh, 1997)

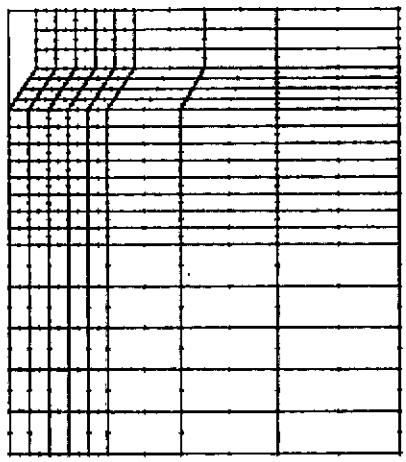

Fig. 2 Finite element mesh for piezocone penetration

analysis and the experiment are presented in the following section and fig. 2 shows the finite element mesh used for the analysis of piezocone penetration.

3. Results of Finite Element Analysis

In this section, the results of the finite element analysis of the piezocone penetration and dissipation tests are compared and investigated with the experimental results. The compared items are cone resistance profile and excess pore water pressure profile during the penetration test, and the change of excess pore water pressure during the dissipation test. In addition, the contours of stress, strain, and excess pore water pressure around the piezocone penetrometer are presented. Sleeve friction was obtained only from the experiments since the finite element analysis was conducted to the penetration depth of maximum 40 mm to avoid tremendous numerical errors. Thus sleeve friction profile is not presented here. For effective presentation of the results, penetration test no.1 in the piezocone penetration test program (table 1) is expressed as 0.3 cm/sec (U1, NC), which means the penetration test conducted using U1 configuration piezocone and normally consolidated sample at the penetration rate of 0.3 cm/sec. Similarly, penetration test no.2, no.3, and no.4 are expressed as 0.3 cm/sec (U2, NC), 0.6 cm/sec (U1, NC), and 0.6 cm/sec (U2, NC), respectively. The 0.6 cm/sec (U2, OCR=10) indicates penetration test no.5. The 0.6 cm/sec (U1, OCR=10) means the test no.6. The U1 configuration is the piezocone with the filter element located at the cone tip and the U2 configuration has the filter element 1mm above the cone base as stated above.

To simulate a real testing situation correctly, it is very important to input correct data. The data for input should reflect the real testing situation and be obtained from the laboratory tests conducted using the same specimens and under the conditions very close to the real situation. The isotropic/anisotropic triaxial compression and creep tests, and oedometer tests have been conducted to obtain the model parameter values of the anisotropic elastoplastic-viscoplastic bounding surface model. The K33 specimen (33% kaolin and 67% fine sand) prepared through the slurry consolidometer technique was used both for the laboratory tests and the piezocone tests conducted using the LSU/CALCHAS. Details on the laboratory tests are described in Kim (1999). The model parameter values in table 2 were used as the input data for the simulations of the penetration test no.1 to no.4 and the model parameter values in table 3 were used for the simulations of the penetration test no.5 and no.6. The following parameter values were commonly used throughout the whole tests: λ=0.06, κ=0.01, Me/Mc=0.8, T=0.05, Re/Rc=0.8, Ae/Ac=0.8, m=0.02, he/hc=1.0, ho=(hc+he)/2, $C_{1e}/C_{1c}=C_{2e}/C_{2c}=C_{3e}/C_{3c}$=1.0, $\Gamma=5\times10^5$, and ε_m=30 %. Details on the parameters are found in Kim (2000).

3.1 Cone Resistance Profiles

The cone resistance was expressed as the corrected cone resistance, q_T, and back pressure, u_o. The corrected cone resistance was obtained from the measured cone resistance and the pore water pressure measured behind the cone tip (Kurup, 1993). The area ratio (λ) of the miniature piezocone used in this research was 0.62. In finite element analyses, cone resistances of U1 and U2 configurations are not differentiable. Pore water pressures, on the other hand, are differentiable. Fig. 3 through fig. 5 show the results of the finite element analyses together with the experimental results. The steady values from the finite element analyses were very close to those obtained experimentally. The steady

Table 2. Model parameter values for test no.1 to no.4

Mc	1 8	s_p	1.0	C_{2c}	1.0
G	15000 KPa	hc	180	C_{3c}	70.0
Rc	1.9	A	1.2	s_v	2.0
Ac	0.1	n_o	1.0	V	5×10^6
C	0.7	C_{1c}	80.0	n	4.0

Table 3. Model parameter values for test no.5 and no.6

Mc	1.8	s_p	1.0	C_{2c}	1.0
G	14500 KPa	hc	130	C_{3c}	70.0
Rc	2.0	A	1.0	s_v	2.0
Ac	0 1	n_o	7.0	V	5×10^6
C	0.7	C_{1c}	80 0	n	4.0

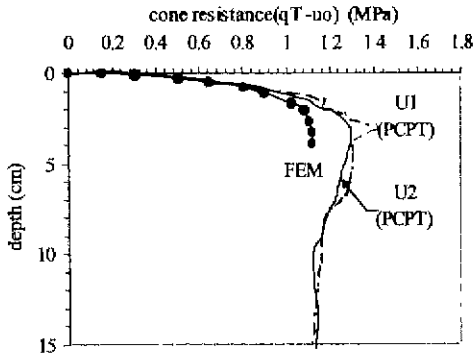

Fig. 3 Cone resistance profiles of NC specimens at 0.3 cm/sec

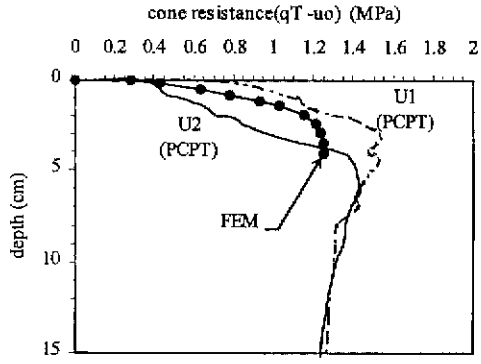

Fig. 4 Con resistance profiles of NC specimens at 0.6 cm/sec

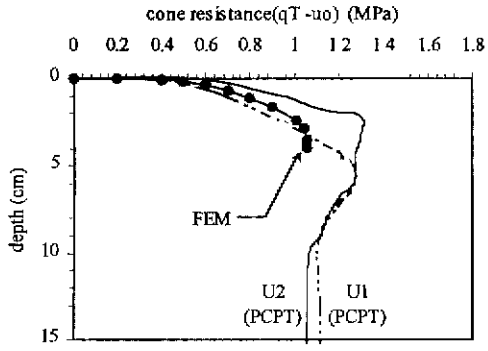

Fig. 5 Cone resistance profiles of OCR =10 specimens at 0.6 cm/sec

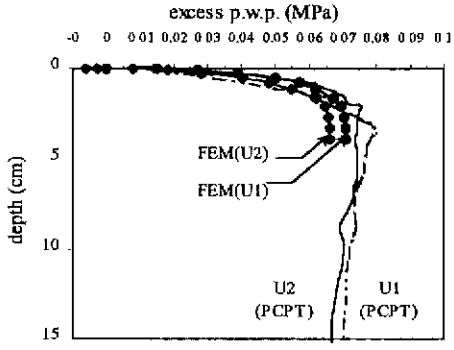

Fig 6 Excess p.w.p. profiles of NC specimens at 0.3 cm/sec

values of cone resistances for 0.6 cm/sec (U1, NC) and 0.6 cm/sec (U2, NC) were almost same (1.23 MPa), and the corresponding penetration depths were also almost same (140 mm). The steady values of cone resistance both for 0.3 cm/sec (U1, NC) and for 0.3 cm/sec(U2, NC) were 1.12 MPa, and the corresponding depths were 105 mm. Accordingly, it can be said that the steady value of cone resistance and the corresponding depth are regardless of the location of filter element. It is because the cone resistances were corrected using the pore water pressure measured behind the cone tip. The steady values of cone resistances for 0.6 cm/sec (U1, OCR=10) and 0.6 cm/sec (U2, OCR=10) were 1.11 MPa and 1.04 MPa, respectively. By comparing the steady values of 0.3 cm/sec (U1 and U2, NC) with those of 0.6 (U1 and U1, NC), it has been found that the cone resistances at higher penetration rate were larger than those at lower rate. In this research, more specifically, the steady value of cone resistance at 0.3 cm/sec increased by 10 % with 100 % increase in penetration rate both for U1 and U2 configurations. By comparing the cone resistances of 0.6 cm/sec (U1 and U2, NC) with those of 0.6 cm/sec (U1 and U2, OCR=10), it has been found that the steady value of cone resistance decreased to 13% with the increase of OCR from 1 to 10 (decrease of effective overburden stress in this research, see table 1).

The cone resistances computed from the finite element analyses reached the steady state conditions at the depth of 30 mm, that is shallower than that of experimental data, as shown in fig. 3 to fig. 5. This disagreement is due to the peak regions, that occurred before the steady state, of the experimental data. These peak regions can be thought as the influence of the thin sand layer at the top of the specimen and occur to initiate the penetrations.

3.2 Excess Pore Water Pressure Profiles

Fig. 6 to fig. 8 show the comparisons of the results of the finite element analyses with the experimental results. The steady values of excess pore water pressures for 0.6 cm/sec (U1, NC), 0.6 cm/sec (U2, NC), 0.3 cm/sec (U1, NC), 0.3

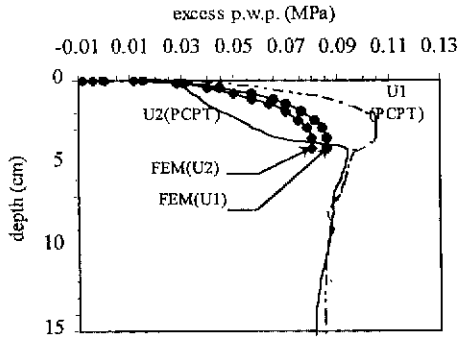

Fig. 7 Excess p.w.p. profiles of NC specimens at 0.6 cm/sec

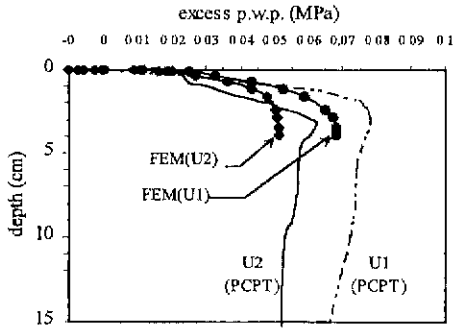

Fig. 8 Excess p.w.p. profiles of OCR=10 specimens at 0.6 cm/sec

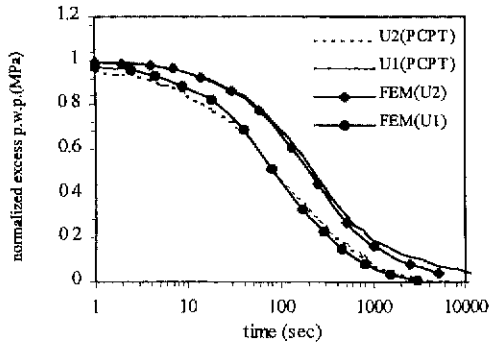

Fig. 9 Excess p.w.p. dissipation of NC specimens at 0.6 cm/sec

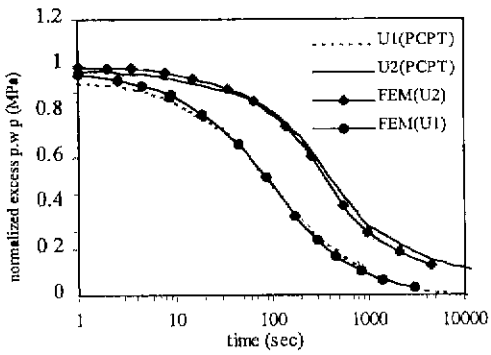

Fig. 10 Excess p.w.p. dissipation of NC specimens at 0.6 cm/sec

cm/sec (U2, NC), 0.6 cm/sec (U1, OCR=10), and 0.6 cm/sec (U2, OCR=10) were 0.086 MPa, 0.081 MPa, 0.067 MPa, 0.064 MPa, 0.063 Mpa, and 0.053 MPa, respectively. In all cases tested under the same stress condition (NC or OCR=10) and at the same penetration rate (0.3 cm/sec or 0.6 cm/sec), it was clearly observed that the excess pore water pressures measured at the cone tip (U1 configuration) were greater than those measured above the cone base (U2 configuration) unlike in the cone resistance profiles. This can be explained by that the soil below the cone tip is subjected to predominantly normal stress, on the other hand, the soil above the cone base mainly experiences shear stress. The differences between the excess pore water pressures of U1 configuration and those of U2 configuration for 0.3 cm/sec (NC), 0.6 cm/sec (NC), and 0.6 cm/sec (OCR=10) were 4.5 %, 5.8 %, and 15.9 %, respectively. So, it can be said that the difference of the excess pore water pressures between U1 and U2 configurations increases with the increase of penetration rate and it also increases with the increase of OCR (decrease of effective overburden pressure in this research). By comparing the excess pore water pressures for 0.3 cm/sec (U1 or U2, NC) with those for 0.6 cm/sec (U1 or U2, NC), with respect to U1 configuration, 22 % increase of excess pore water pressure has been found with the increase of penetration rate from 0.3 cm/sec to 0.6 cm/sec. With respect to U2 configuration, 21 % increase of excess pore water pressure has been found with the increase of penetration rate from 0.3 cm/sec to 0.6 cm/sec. This means that excess pore water pressures measured both at the cone tip and above the cone base increase with the increase of penetration rate at a very similar rate. By comparing the results of 0.6 cm/sec (U1 and U2, NC) with those of 0.6 cm/sec (U1 and U2, OCR=10), the 27 % and 33 % decreases of excess pore water pressures have been found with the increase of OCR from 1 to 10 for U1 and U2 configurations, respectively, which means the decrease of excess pore water pressure in U2 configuration is greater than that in U1 configuration with the increase of OCR (decrease of effective overburden pressure in this research). With respect to excess pore water pressure, U1 and U2 configurations

should be differentiated in finite element analyses as well as in experimental results. The steady values of excess pore water pressures computed numerically were quite close to those obtained experimentally. The excess pore water pressures obtained from finite element analyses reached the steady state conditions at the depth of 30 mm, which are shallower than those of experimental data. This behavior in excess pore water pressure profiles is similar to that in cone resistance profiles. This disagreement is due to the peak regions of the experimental results, which are the influence of the thin sand layer at the top of the specimen and are needed to initiate penetrations. It is interesting to note that negative pore water pressures were likely to develop above the cone base at the early stage of the penetration. It is due to the soil-piezocone separation near the cone base, so an appropriate simulation of the peak region and the separation is needed in future research.

3.3 Dissipation of Excess Pore Water Pressure

In fig. 9 through fig. 11, the dissipation results from the experiments are compared with the results from finite element analyses. The excess pore water pressures were normalized by their initial excess pore water pressures, which are the excess pore water pressures when the penetrations stopped for the dissipation tests. The dissipations of excess pore water pressures in NC cases took longer time than those in OCR=10 cases both for the U1 and U2 configurations. However, the biggest difference of all dissipation curves is their initial values, i.e., the leftmost values are not unity in fig. 9 through fig. 10. These initial

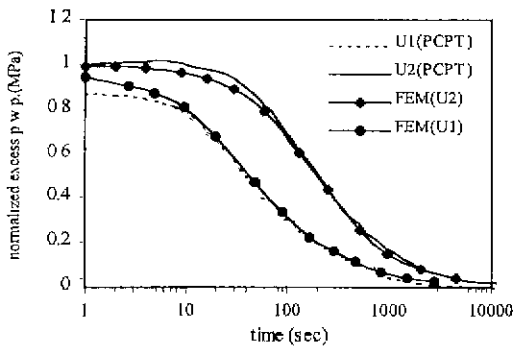

Fig. 11 Excess p.w.p. dissipation of OCR=10 specimen (0.6 cm/sec)

drops were higher for the pore water pressures measured at the cone tip (U1 configuration) than those measured above the cone base (U2 configuration). It is due to the redistribution of pore water pressure and the normal stress reduction that occurs when the penetration ceases (Tumay, et al., 1995). It has been also found that the magnitude of the initial drop increased with the increase of the penetration rate, and that the excess pore water pressure increased, a little bit, immediately after the initial drop for the case of 0.6 cm/sec (U2, OCR=10). It is obvious that the numerical results are quite close to the experimental results with the exception of the initial drops. It was observed that the cases that had relatively big initial drops, i.e., 0.6 cm/sec (U1, NC) and 0.6 cm/sec (U1, OCR=10), showed disagreement with the experimental data for the initial parts of dissipation curves. So, an appropriate simulation for the initial drop is needed for future research. The current finite element analyses, however, gave good results in steady values of cone resistance and excess pore water pressure, and dissipation since the elastoplastic-viscoplastic bounding surface model was used.

3.4 Contours of Stress, Strain, and Excess Pore Water Pressure

Fig. 12 shows the contours of the octahedral shear stresses, that have been obtained from the finite element analyses, around the piezocone penetrometer at the penetration depth of 30 mm for 0.3 cm/sec (U1 and U2, NC), 0.6 cm/sec (U1 and U2, NC), and 0.6 cm/sec (U1 and U2, OCR=10), respectively. The vertical and radial distances were normalized by the radius of the piezocone penetrometer, r_o. For 0.3 cm/sec (U1 and U2, NC), the maximum octahedral shear stress was 122 KPa and it was concentrated both on the lower and the upper portions of the conical face. For 0.6 cm/sec (U1 and U2, NC) and 0.6 cm/sec (U1 and U2, OCR=10), the maximum octahedral shear stresses were 153 KPa and 121 KPa, respectively, and they were also concentrated both on the lower and the upper portions of the conical face. The magnitude of the octahedral shear stress and the affected zone increased, as expected, with the increase of penetration rate, but they decreased with

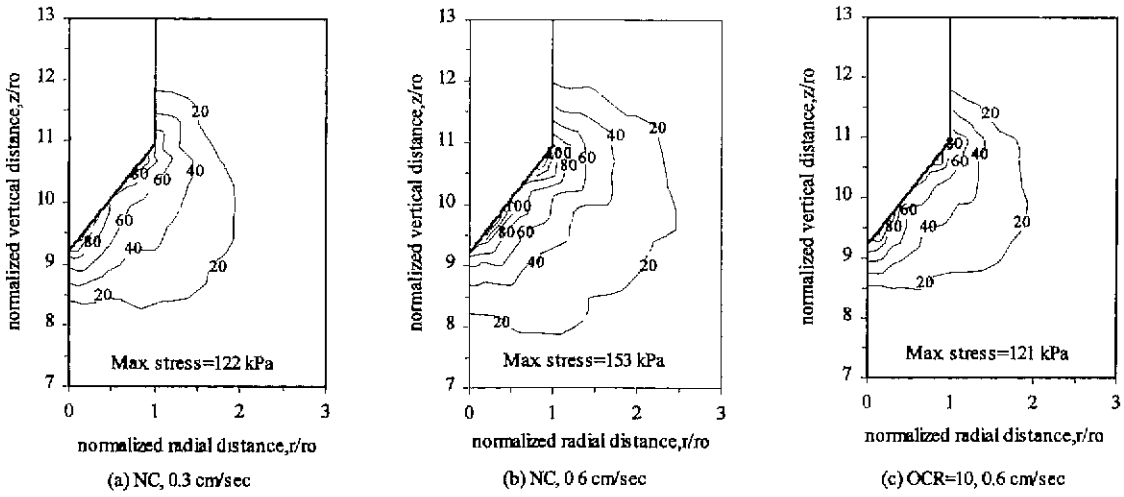

Fig. 12 Octahedral shear stress contours at 30 mm depth

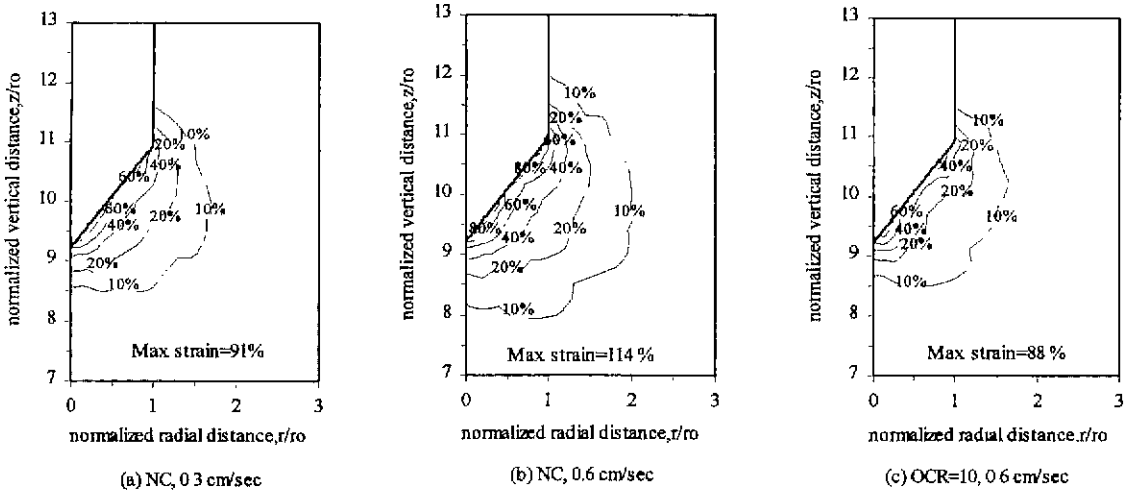

Fig. 13 Octahedral shear strain contours at 30 mm depth

the increase of OCR (decrease of effective overburden pressure in this research). It has been also found that the octahedral shear stresses changed very rapidly above the cone base for all cases, and the affected shearing zone for the overconsolidated case, 0.6 cm/sec (U1 and U2, OCR=10), was localized in a smaller zone than that for the normally consolidated case, 0.6 cm/sec (U1 and U2, NC).

Fig. 13 shows the contours of the octahedral shear strains around the piezocone penetrometer at the penetration depth of 30 mm for 0.3 cm/sec (U1 and U2, NC), 0.6 cm/sec (U1 and U2, NC), and 0.6 cm/sec (U1 and U2, OCR=10), respectively. The vertical and radial distances were normalized by the radius of the piezocone penetrometer, r_o. The shapes and the trends of the octahedral shear strain contours with respect to the penetration rate and the value of OCR were very similar to those of the octahedral shear stress contours. For 0.3 cm/sec (U1 and U2, NC), the maximum octahedral shear strain was 91 % and it was concentrated both on the lower and the upper portions of the conical face. For 0.6 cm/sec (U1 and U2, NC) and 0.6 cm/sec (U1 and U2, OCR=10), the maximum octahedral shear strains were 114 % and 88 %, respectively, and they were also concentrated both on the lower and the upper portions of the conical face. The calculated strains were quite large.

This demonstrates the need of using a large deformation finite strain formulation. The magnitude of the octahedral shear strain and the affected zone increased, as expected, with the increase of penetration rate, but they decreased with

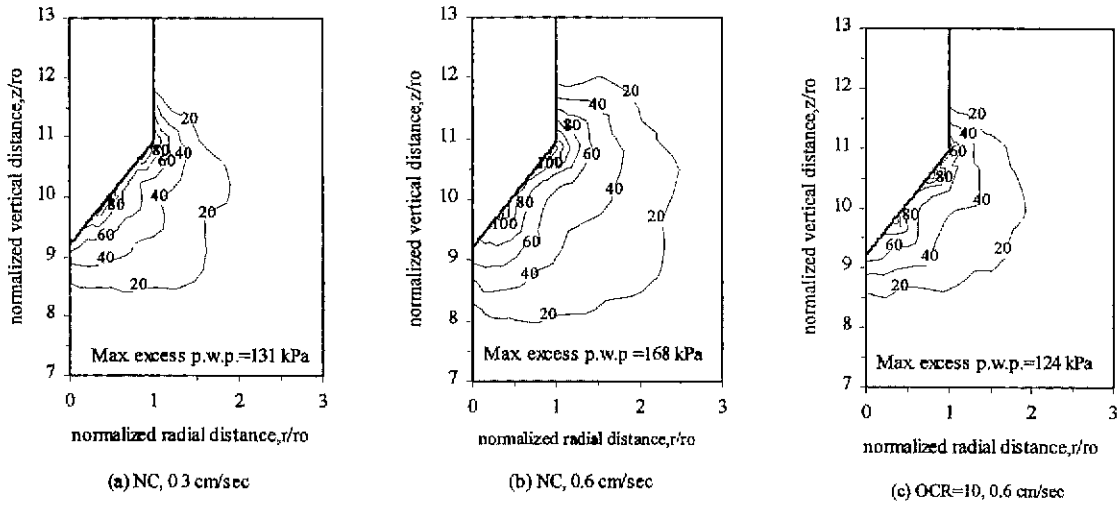

Fig. 14 Excess pore water pressure contours at 30 mm depth

the increase of OCR (decrease of effective overburden pressure in this research). It has been also found that the octahedral shear strain for the overconsolidated case, 0.6 cm/sec (U1 and U2, OCR=10), was localized in a smaller zone than that for the normally consolidated case, 0.6 cm/sec (U1 and U2, NC), like in the octahedral shear stress.

The contours of the excess pore water pressures developed around the piezocone penetrometer at the penetration depth of 30 mm are presented in fig. 14. It has been observed that the shapes and the trends of the excess pore water pressure contours with respect to the penetration rate and the value of OCR were very similar to those of the octahedral shear stress contours. The maximum excess pore water pressures were 131 KPa for 0.3 cm/sec (U1 and U2, NC), 168 KPa for 0.6 cm/sec (U1 and U2, NC), and 124 KPa for 0.6 cm/sec (U1 and U2, OCR=10). Like in the contours of the octahedral shear stresses, the excess pore water pressures were concentrated both on the lower and the upper portions of the conical face for 0.3 cm/sec (U1 and U2, NC), 0.6 cm/sec (U1 and U2, NC), and 0.6 cm/sec (U1 and U2, OCR=10). It can be said that the magnitude of the excess pore water pressure and the affected zone increased with the increase of penetration rate, but they decreased with the increase of OCR (decrease of effective overburden pressure in this research). The excess pore water pressures at the cone tip (U1) and above the cone base (U2) were quite different, and the excess pore water pressure above the cone base changed very rapidly for all cases, which produced a large pore pressure gradient. So, the location of the filter element for measuring excess pore water pressure needs to be emphasized again. It has been also found that the affected shearing zone for the overconsolidated case, 0.6 cm/sec (U1 and U2, OCR=10), was localized in a smaller zone than that for the normally consolidated case, 0.6 cm/sec (U1 and U2, NC).

4. Conclusions

In this research, the finite element analyses of the miniature piezocone penetration and subsequent dissipation tests were conducted using the elastoplastic-viscoplastic bounding surface model and the Updated Lagrangian formulation to consider the large strain nature of the piezocone penetration. The results of the finite element analyses were compared with the experimental results of the piezocone penetration and dissipation tests conducted using LSU/CALCHAS (Louisiana State University Calibration Chamber System). The finite element analysis and the experiments have been conducted for U1 and U2 piezocone penetrometers, for normally consolidated and heavily overconsolidated cohesive specimens, and at the penetration rates of 0.3 and 0.6 cm/sec. The results of the finite element analyses showed very good agreement with the experimental data for the profiles of cone resistance, excess pore water pressure, and for dissipations. Incorporation of the anisotropic elastoplastic -viscoplastic soil model and a large deformation and finite

strain formulation provided this improvement. The following conclusions can be made.

The steady values of cone resistance and excess pore water pressure from the finite element analyses were very close to the values obtained experimentally. The cone resistance and the excess pore water pressure computed numerically reached the steady state conditions at the depth of 30 mm, that was shallower than that of experimental results. This disagreement is due to the boundary induced peak regions, which occurred before the steady state, of the experimental results. This peak region can be thought to be the influence of the thin sand layer at the top of the specimen and prior to penetration initiation. It was observed that negative pore water pressures from the finite element analyses were likely to develop above the cone base at early stages of penetration. It may be due to the soil-piezocone separation near the cone base in finite element analyses. The results of the finite element analyses for the dissipations were very good except the cases with high immediate initial drop, i.e., the cases of U1 configurations and the high penetration rate (0.6 cm/sec, NC and OCR=10).

Octahedral shear stresses, octahedral shear strains, and excess pore water pressures were concentrated both on the lower and the upper portions of the conical face for 0.3 cm/sec (U1 and U2, NC), 0.6 cm/sec (U1 and U2, NC), and for 0.6 cm/sec (U1 and U2, OCR=10). The magnitudes and the affected zones of octahedral shear stress, octahedral shear strain, and excess pore water pressure increased with the increase of penetration rate, but decreased with the increase of OCR (decrease of effective overburden pressure in this research). Octahedral shear strains computed numerically were quite large, i.e., the maximum values were 91 %, 114 %, and 88 % for 0.3 cm/sec (U1 and U2, NC), 0.6 cm/sec (U1 and U2, NC), and 0.6 cm/sec (U1 and U2, OCR=10), respectively. This demonstrates the need of using a large deformation finite strain formulation.

Acknowledgments

The financial support for the work described in this paper was provided through a grant CMS-9531782 by NSF. The writers acknowledge Professor Mehmet T. Tumay, Professor George Z. Voyiadjis, and Dr. Abu-Farsakh.

References

1 Abu-Farsakh, M. Y., Voyiadjis, G. Z., and Tumay, M T. (1997), "Numerical Analysis of the Miniature Piezocone Penetration Tests (PCPT) in Cohesive Soils." International Journal for Numerical and Analytical Methods on Geomechanics (In Press)

2. Al-Shamrani, M. A. and Sture, S. (1994), "Characterization of Time-dependent Behavior of Anisotropic Cohesive Soils," Computer Methods and Advances in Geomechanics, Siriwardane & Zaman (eds), pp. 505-511

3. Katona, M. G. (1983), "A Simple Contact-Friction Interface Element with Applications to Buried Culverts," International Journal for Numerical and Analytical Methods in Geomechanics, Vol. 7, pp. 371-384

4. Kim. D.-K. (1999), "Numerical Simulation and Experimental Verification of Cone Penetration Rate and Anisotropy in Cohesive Soils," Ph.D. Dissertation, Dept. of Civil and Environmental Engineering, Louisiana State University, Baton Rouge, LA. 211 pp.

5. Kim, D.-K. (2000), "A Study on the Model Parameters of the Anisotropic Elastoplastic-viscoplastic Bounding Surface Model for Cohesive Soils," Journal of the Korean Geotechnical Society, Vol 17, No. 3

6. Kurup, P. U. (1993), "Calibration Chamber Studies of Miniature Piezocone Penetration Tests in Cohesive Soil Specimens," Ph. D. Dissertation, Department of Civil and Environmental Engineering, Louisiana State University, Baton Rouge, LA. 234 pp

7. Prevost, J. H. (1980), "Mechanics of Continuous Porous Media," International Journal of Engineering Science, Vol. 18, pp. 787-800

8. Tumay, M. T., Kurup, P. U., and Voyiadjis, G. Z. (1995), "Profiling OCR and Ko from Piezocone Penetration Tests." International Symposium on Cone Penetration Testing, Sweden. pp 337-342.

9. Voyiadjis, G. Z. and Abu-Farsakh, M. Y. (1997), "Coupled Theory of Mixtures for Clayey Soils," Computers and Geotechnics, Vol. 20, No.3/4, pp. 195-222

(접수일자 2000. 5. 10)